Optimal Control Based Vertical Trajectory Determination for Continuous Descent Arrival Procedures

Sang Gyun Park* and John-Paul Clarke†
Georgia Institute of Technology, Atlanta, Georgia 30332

DOI: 10.2514/1.C032967

Continuous descent arrival (CDA) procedures provide time and fuel savings, and reduce the noise impact of aircraft operations near airports. To date, these procedures have been designed to limit the performance envelopes to achieve trajectory commonality. In this paper, the performance bounds of CDA procedure via multiphase optimal vertical trajectory generation problems with respect to two performance indices — flight time and fuel consumption — have been investigated. The optimal CDA vertical profile is first divided into two segments: the cruise segment before the top of descent (TOD) and the descent segment from the TOD. Then, the second segment is further subdivided based on flap setting and speed constraints. Finally, the resulting multiphase optimal control problem is solved using a pseudospectral method. Two different types of aircraft, B737-500 (light) and B767-400 (heavy), are used in a numerical study, and the optimal CDA trajectories of the two types are compared with a typical vertical navigation (VNAV) CDA trajectory used in CDA applications at several airports. Then, the utility of suboptimal VNAV CDA trajectories that can be created with known flight management system (FMS) VNAV descent modes is explored, and thereby enabling onboard calculation in the FMS via the sensitivity analysis that is performed with various wind conditions.

Nomenclature

D	=	drag force
h	=	altitude
L	=	lift force
M	=	Mach number
m	=	aircraft mass
p	=	phase index
T	=	thrust force
V_{CAS}	=	calibrated airspeed
V_G	=	ground speed
V_T	=	true airspeed
$\boldsymbol{W}$	=	wind-velocity vector
W_c	=	cross component of the wind velocity
W_h	=	horizontal component of the wind velocity
x_s	=	along-track distance
γ	=	aerodynamic flight path angle
ψ	=	heading angle
ψ_w	=	angle between heading direction and airspeed in the horizontal plane

I. Introduction

NOISE-ABATEMENT arrival and approach procedures are used to reduce the impact of aircraft-related noise in communities near airports. Among the several noise-abatement procedures that have been studied, the continuous descent arrival (CDA) has been applied at several airports, and has been shown to be an effective way of achieving reductions in noise [1–3]. CDA has been shown to reduce the operating costs, such as the fuel consumption and the flight time during the arrival procedure [2,3]. Because an aircraft that performs a CDA descends continuously from its top of descent (TOD) with its engines at or near idle power and with no level-flight segment at low altitudes, it reduces the noise impact in communities near airports. Additionally, due to the resulting higher airspeeds closer to the runway and the lower fuel burn rate at idle thrust, CDAs reduce both flight time and fuel burn. In spite of these benefits, the widespread implementation of CDAs has been limited because air traffic controllers (ATCs) have difficulty predicting descent trajectories at idle thrust that vary widely according to aircraft types and wind conditions. This difficulty leads to an unnecessarily large separation between aircraft, and degrades throughput in the Terminal Radar Approach Control (TRACON) area.

This concern may be addressed by computing the required minimum separation between aircraft performing a CDA. Ren and Clarke [4] developed the tool for analysis of separation and throughput for this purpose, and demonstrated its utility via flight test [5]. Another approach to handle the throughput issue in TRACON is to assign a required time of arrival (RTA) at a meter fix for each aircraft. The RTA assignment at a meter fix requires a CDA performance-bound analysis of individual aircraft for the feasible operation. For this reason, ATCs need a methodology to analyze the performance bound of the CDA trajectory depending on the aircraft types and wind conditions.

An optimal control framework is useful to analyze the performance bound of the trajectory. Therefore, to maximize the benefits of the CDA procedure and to study the performance bound of a CDA trajectory, we develop and examine the trajectory optimization of the CDA procedure in the optimal control framework. Several methods have been proposed for trajectory optimization. Erzberger and Lee [6] proposed a trajectory-optimization scheme for a fixed range in terms of direct operating cost, which is the combined cost of fuel and flight time. Sorensen and Waters [7] proposed an airborne fuel optimal flight-trajectory-generation method to meet the assigned time of arrival. Burrows [8] proposed an onboard fuel optimal-trajectory-generation method for fixed-time and fixed-range flight. Chakravarty [9] proposed a fuel optimal en route descent trajectory, including the cruise segment. In these studies [6–9], simplified energy state equations that use energy as the independent variable instead of time were used as aircraft dynamics equations, reducing the problem size. However, operating requirements, such as flap extension and speed limits, were ignored. Visser and Wijnen [10] described a multiphase optimal control problem with respect to community noise impact in the vicinity of airports. In this research, optimal results were obtained for aircraft operations below 10,000 ft by using awakening as a performance index. Slattery and Zhao [11] proposed a trajectory-synthesis method with a predetermined

Presented as Paper 2012-4757 at the AIAA Guidance, Navigation, and Control Conference, Minneapolis, MN, 13–16 August 2012; received 25 April 2014; revision received 10 October 2014; accepted for publication 11 October 2014; published online 20 January 2015.

*Ph.D. Student, School of Aerospace Engineering, 270 Ferst Drive Northwest. Student Member AIAA.

†Associate Professor, School of Aerospace Engineering, 270 Ferst Drive Northwest. Associate Fellow AIAA.

sequence of vertical area navigation (VNAV) functions for the en route descent phase by using their own capture-condition analysis of each VNAV mode [12]. However, this trajectory is not optimal.

In this paper, we present optimal CDA trajectories that maximize the benefits in terms of operating costs, such as fuel consumption or flight time. The performance bound of a CDA trajectory is determined by the two optimal trajectories [13]. Idle power is assumed during the descent. To obtain these optimal trajectories, we formulate problems as multiphase optimal control problems with a fixed range, and consider both operating conditions and speed constraints. The altitude range considered in this paper is from the cruise altitude to the intercept of the Instrument Landing System (ILS) glide slope. By dividing the optimal trajectory into two flight segments, cruise and descent, we simultaneously obtain both the position of the TOD and the subsequent optimal descent path. Furthermore, we propose suboptimal trajectories for a VNAV CDA based on the optimal-trajectory results. The proposed VNAV CDA vertical profiles can be calculated by an onboard flight management system (FMS) computer without additional equipment, and the numerical results show that the performance of the proposed profiles is very similar to the optimal results.

The remainder of this paper is organized as follows. In Sec. II, we formulate a multiple-phase Bolza optimal control problem for CDA. In Sec. III, we provide numerical-optimization results and sensitivity analyses of the optimal trajectories for the B737-500 (B737) and B767-400 (B767). In Sec. IV, we propose two suboptimal VNAV CDA trajectories, which are constructed using the existing VNAV descent algorithms in the FMS: idle-thrust constant calibrated airspeed (CAS)/Mach descent, constant rate of descent (ROD), and constant flight path angle (FPA). In Sec. V, we summarize and present the conclusions of this study.

II. Optimal Control Problem Formulation

A. Flight Dynamics Model

The dynamic model of the aircraft greatly influences the optimization results, and an accurate model is necessary to obtain realistic results. While a high-order dynamics model can capture accurate aircraft behaviors, a simplified dynamics model, on the other hand, can reduce computational time by reducing the order of equations. After considering this tradeoff, we decided to use a three-dimensional point mass flight dynamics model, in which moment equations are ignored by assuming that the attitude of the aircraft is controlled by an autopilot. Therefore, only force equations are used to describe the aircraft's vertical and lateral motions. To derive the equations of motion, we use the following two assumptions: 1) the mass of the aircraft remains constant during the arrival procedure; and 2) the wind vector $\boldsymbol{W}$ is a function of altitude. The first assumption, which results in us ignoring the effect of mass changes, is quite reasonable because the fuel consumption during the arrival procedure is below 0.5% of the total mass [2]. In addition, the lateral path of the arrival procedure is given by published Standard Terminal Arrival Route (STAR); we only consider the vertical dynamics. Therefore, we use the along-track distance x_s instead of the x and y positions. The equations of motion used in this paper are as follows [14]:

$$\dot{V}_T = \frac{1}{m}(T - D) - g \sin\gamma - \frac{1}{2} V_T \sin 2\gamma \left(\frac{\mathrm{d}U_w}{\mathrm{d}h} \cos\chi + \frac{\mathrm{d}V_w}{\mathrm{d}h} \sin\chi \right) \tag{1}$$

$$\dot{x}_s = \sqrt{(V_T \cos\gamma)^2 - W_c^2} + W_h \tag{2}$$

$$\dot{h} = V_T \sin\gamma \tag{3}$$

in which the state variables V_T, x_s, and h are true airspeed, along-track distance, and altitude; γ is the aerodynamic FPA; T and D are thrust and drag forces; and $W_c = \boldsymbol{W} \sin(\Psi_w - \psi)$ and $W_h = \boldsymbol{W} \cos(\Psi_w - \psi)$ are the cross- and horizontal-wind components, respectively. The relations between heading angle, ground speed, and wind vector are described in Fig. 1.

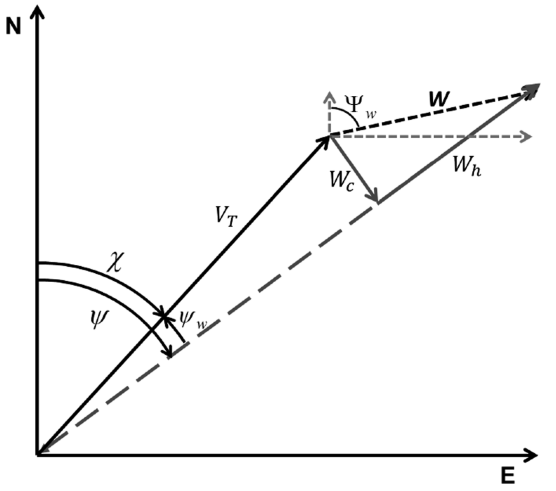

Fig. 1 Relation between airspeed, ground speed, and wind vector.

B. CDA Trajectory Structure

In this paper, the flight range covers some portion of the cruise segment, which is from an initial waypoint to the TOD, and a flight idle-descent segment, which is from the TOD to the initial approach fix (IAF), as shown in Fig. 2. In the first segment, which is the cruise segment, it is assumed that the aircraft flies at its cruise altitude at a constant airspeed. The second segment is from the TOD point to a final point, in other words, the termination point of the CDA procedure. In this segment, the aircraft descends continuously at flight idle thrust, and flaps are extended in accordance with the aircraft specific flap-speed schedule as specified by the airframe manufacturer. While the maximum and minimum airspeeds for each flap setting are defined to prevent any structural damage and provide a stall margin, respectively, the flap-extension speed can be optimized within the speed bound of two adjacent flap settings [15]. However, in this chapter, to reflect what is done in actual operation, we use a specific flap-extension speed within the speed bound for each flap extension, as is typically the case in commercial air carrier operations.

Because the drag-polar curve varies with flap setting, the aircraft dynamics changes, and it is therefore necessary to distinguish the phase based on flap setting. In addition, an interior-point constraint is required due to the Federal Aviation Administration (FAA) speed limitation, which limits aircraft to an indicated airspeed (IAS) of 250 kt at or below 10,000 ft. To handle such an interior-point constraint, it is necessary to distinguish the phase before and after the interior-point constraint even though flaps are not extended. For this reason, as shown in Fig. 2, the second segment is divided into several

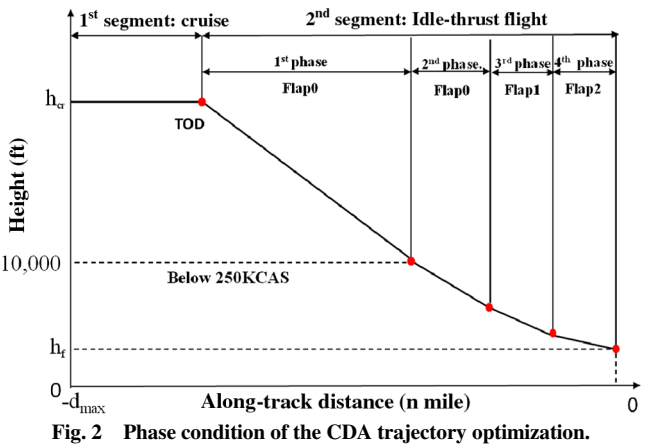

Fig. 2 Phase condition of the CDA trajectory optimization.

separate phases. The first phase is from the TOD point to an altitude of 10,000 ft. The subsequent phases start from the 10,000 ft altitude, and are separated at the points where the aircraft reaches each required flap-extension speed. Each segment of a flap extension and its associated speed depends on the aircraft types and weights. The final phase terminates upon the aircraft reaching the final point of the CDA procedure.

An example of the required phases for three segments of a flap extension is shown in Fig. 2. According to the segment and phase split in Fig. 2, we can define the performance index and various constraints to formulate a CDA trajectory-optimization problem.

C. Multiphase Optimal Control Problem Formulation

A multiphase optimal control problem formulation may be used to consider the CDA trajectory structure in Fig. 2. To obtain a realistic trajectory, we consider several practical constraints, such as the speed limitation of FAA regulation 91.117 and aircraft operating constraints, including their flap-speed schedule. The general formulation of a multiphase optimal control problem is as follows:

$$J = \sum_{p=1}^{N}\left[\Phi^{(p)}(x_0^{(p)}, t_0^{(p)}, x_f^{(p)}, t_f^{(p)}) + \int_{t_0^{(p)}}^{t_f^{(p)}} L^{(p)}(x^{(p)}, u^{(p)}, t)\,\mathrm{d}t\right] \quad (4)$$

subject to the dynamic constraint

$$\dot{x}^{(p)} = f^{(p)}(x^{(p)}, u^{(p)}, t) \quad (5)$$

subject to the event constraint of each phase

$$\phi_{\min}^{(p)} \le \phi(x_0^{(p)}, t_0^{(p)}, x_f^{(p)}, t_f^{(p)}) \le \phi_{\max}^{(p)} \quad (6)$$

subject to the path constraint

$$g_{\min}^{(p)} \le g^{(p)}(x^{(p)}, u^{(p)}, t) \le g_{\max}^{(p)} \quad (7)$$

subject to phase link constraint

$$P^{(s)}(x_f^{(p-1)}, t_f^{(p-1)}, x_0^{(p)}, t_0^{(p)}) = 0 \quad (8)$$

in which N is the number of phases; and $\Phi^{(p)}$ and $L^{(p)}$ are the Mayer cost and Lagrangian of the pth phase, respectively. The detailed description of each component in Eqs. (4–8) will be explained in the subsequent subsections.

1. Performance Index

The CDA procedures provide significant benefits relative to a conventional arrival/approach with level-flight segments. In addition to the noise reduction, the CDA procedures enable reductions in fuel consumption and flight time [2]. To maximize the benefits of a CDA, the fuel consumption and flight time for the fixed-range CDA were selected as the performance indices. Further, the idle-power condition ensures that the noise impact is minimized if the other two are minimized. Thus, we choose fuel consumption and flight time for the CDA as the performance indices.

Through the paper, the wind is assumed to be a function of altitude, which means that wind speed is constant at the same altitude regardless of the lateral position. From this assumption, the performance indices can be expressed as the following simple formulations: 1) flight-time performance index

$$\begin{aligned} J &= \Phi^{(1)}(x_s^{(1)}(t_0), V_t^{(1)}(t_0)) + t_f^{(N)} \\ &= \underbrace{(x_s^{(1)}(t_0) - d_{\max})/V_G^{(1)}}_{\text{first-segment flight time}} + \underbrace{t_f^{(N)}}_{\text{second-segment flight time}} \end{aligned} \quad (9)$$

and 2) fuel-consumption performance index

$$\begin{aligned} J &= \Phi^{(1)}(x_s^{(1)}(t_0), V_T^{(1)}(t_0), h^{(1)}(t_0)) + \sum_{p=1}^{N}\int_{t_0}^{t_f^{(p)}} L^{(p)}\,\mathrm{d}t \\ &= \underbrace{\dot{f}_{\mathrm{cr}} \times (x_s^{(1)}(t_0) - d_{\max})/V_G^{(1)}}_{\text{first-segment fuel consumption}} + \underbrace{\sum_{p=1}^{N}\int_{t_0}^{t_f^{(p)}} \dot{f}_d^{(p)}\,\mathrm{d}t}_{\text{second-segment fuel consumption}} \end{aligned} \quad (10)$$

in which $d_{\max}$, $\dot{f}_{\mathrm{cr,cruise}}$, and $\dot{f}_{\mathrm{cr}}$ are the maximum range, fuel flow rate at cruise at a given cruise speed, and idle-thrust fuel flow rate, respectively.

As shown in Eqs. (9) and (10), both the flight-time and fuel-consumption performance indices are divided into two parts: one for each segment. The first Mayer cost represents a cost during the cruise segment, and the second cost term is for the flight idle-descent segment.

By defining the performance index in two parts, as shown previously, with the free TOD condition, we can transform a fixed-range optimal control problem into a free initial-condition optimal control problem. Hence, we can obtain both the optimal TOD point and the optimal vertical trajectory for the CDA procedures regarding both minimum flight time and minimum-fuel consumption. Furthermore, $d_{\max}$ does not affect the optimal TOD point and vertical profile from the following lemma.

Lemma 1: Let us assume that the optimal solution with respect to the performance index in Eq. (9) or (10) exists with a given $d_{\max}$, which is farther than $\mathrm{TOD}_{\mathrm{opt}}$ from the runway threshold. Consider the optimal-solution pair $(\mathrm{TOD}_{\mathrm{opt}_1}, u_{\mathrm{opt}_1})$ associated with $d_{\max_1}$. Then, the optimal-solution pair $(\mathrm{TOD}_{\mathrm{opt}_2}, u_{\mathrm{opt}_2})$ associated with a different $d_{\max_2}$ is the same as $(\mathrm{TOD}_{\mathrm{opt}_1}, u_{\mathrm{opt}_1})$ if $d_{\max_2}$ is farther than $\mathrm{TOD}_{\mathrm{opt}_1}$ from the runway threshold.

Proof: The TOD $x_s^{(1)}(t_0)$ is limited by $d_{\max}$ as

$$d_{\max} \le x_s^{(1)}(t_0) \quad (11)$$

We can express performance indices in Eqs. (9) and (10) as follows:

$$J = J_1 + J_2 \quad (12)$$

in which J_1 is the Mayer cost, and J_2 is the Lagrange cost. J_1 is a function of $d_{\max}$ and TOD $x_s^{(1)}(t_0)$. Furthermore, J_1 is expressed as a summation of the TOD term $J_{1,\mathrm{TOD}}$ and $d_{\max}$ term $J_{1,d_{\max}}$. Therefore, J in Eqs. (9) and (10) can be rewritten as

$$J = J_{1,d_{\max}} + J_2(\mathrm{TOD}, u) \quad (13)$$

in which $J_2(\mathrm{TOD}, u) = J_{1,\mathrm{TOD}} + J_2$. If $d_{\max}$ is given, $J_{1,d_{\max}}$ is a constant. Therefore, the original problem is equivalent to the problem with $J_2(\mathrm{TOD}, u)$, which is independent to $d_{\max}$. For this reason, $(\mathrm{TOD}_{\mathrm{opt}_2}, u_{\mathrm{opt}_2}) = (\mathrm{TOD}_{\mathrm{opt}_1}, u_{\mathrm{opt}_1})$ if both $\mathrm{TOD}_{\mathrm{opt}_{1,2}}$ are interior points of Eq. (11). □

Remark 1: Lemma 1 provides the condition for setting $d_{\max}$. The $d_{\max}$ value should be farther from the runway threshold than the optimal TOD. Because x_s at the runway threshold is zero, and $d_{\max}$ is always negative, farther from the runway threshold means a smaller value. We should select the smaller value if $d_{\max} = \mathrm{TOD}_{\mathrm{opt}}$.

Remark 2: Lemma 1 implies that the $d_{\max}$ value that satisfies Eq. (11) does not affect the optimal solution. We can select any $d_{\max}$ from $\mathrm{TOD}_{\mathrm{opt}}$ as the starting point of the cruise phase. Therefore, the optimal solution can include all flight segments except climb. However, the initial waypoint must not be too far from the runway threshold because the aircraft mass is assumed to be a constant during the CDA procedure, which includes some portion of cruise, as shown

in Fig. 2. Therefore, this fact gives the minimum limit of the $d_{\max}$ value.

2. Constraints for the CDA

To obtain a realistic trajectory resulting from the optimal control problem, we should consider operating conditions, such as the flap-speed schedule, landing-gear extension, regulated speed restrictions, and bounded control-input constraints. These conditions can be expressed as specific constraints in Eqs. (6–8). The following are constraints implemented in the optimal control problem for a CDA: 1) event constraint of each phase

$$d_{\max} \le x_s^{(1)}(t_0) \tag{14}$$

$$V_{\mathrm{CAS}}^{(1)}(t_f) \le 250 \text{ kt} \tag{15}$$

$$V_{\mathrm{CAS}}^{(p)}(t_f) = V_{F(p)}, \quad \text{for } p = 2, 3, \ldots, N \tag{16}$$

2) path constraints of each phase

$$V_{\mathrm{min,CAS}}^{(p)} \le V_{\mathrm{CAS}}^{(p)}(t) \le V_{\mathrm{max,CAS}}^{(p)} \tag{17}$$

$$\dot{h}_{\min} \le \frac{\mathrm{d}h}{\mathrm{d}t} \le \dot{h}_{\max} \tag{18}$$

$$M_{\min}^{(p)} \le M^{(p)}(t) \le M_{\max}^{(p)} \tag{19}$$

3) phase link constraints

$$\boldsymbol{x}^{(p-1)}(t_f) = \boldsymbol{x}^{(p)}(t_0) \tag{20}$$

and 4) input constraint

$$\gamma_{\min} \le \gamma \le \gamma_{\max} \tag{21}$$

Equation (15) is formulated to meet the FAA regulation that limits the maximum allowable CAS speed to 250 kt below 10,000 ft. Equation (16) implies that the speed at the end of the phase should be the same as the next flap-extension speed, in which $V_{F(p)}$ is the flap-extension speed to the $F(p)$ setting.

Equation (17) constrains the aircraft CAS to be between the published maximum and minimum flap-extension speeds. Equation (18) restricts the descent rate to the maximum established for passenger comfort and the minimum to prevent level flight, and also to restrict deceleration performance. Usually, the flight envelope is restricted by both the CAS and the Mach number. Therefore, avoiding a violation of the flight envelope can be accomplished by using Eqs. (17) and (19) as path constraints.

Table 1 Flap-speed schedules of B737 and B767 (CAS)

	B737			B767		
Flap mode	Flap0	Flap1	Flap2	Flap0	Flap1	Flap2
Angle, deg	0	1	5	0	5	15
Extension, kt	— —	210	190	— —	230	190
Minimum CAS, kt	210	190	180	230	190	170

To ensure state variables remain continuous, we add the phase link constraint in Eq. (20). Because we assume idle power during the second segment of the optimal trajectory, the aerodynamic FPA is the only control input. Equation (21) imposes a limit on the aerodynamic FPA.

III. Trajectory Optimization Results for CDA

In this section, we present the trajectory-optimization results for a CDA in the vertical plane. As mentioned in Sec. II, a wind vector is assumed to be a function of altitude only. We consider both horizontal- and cross-wind components. Because the lateral path is given by STAR, we focus on vertical motion only.

As seen in Sec. II, the equations of motion are nonlinear differential equations; both drag and lift-force vectors are nonlinear functions of air density, airspeed, and altitude. Furthermore, many constraints with respect to IAS have a nonlinear relationship with true airspeed [16], making it difficult to solve the problem analytically. For this reason, we use a numerical-optimization technique. A pseudospectral method is chosen for this problem to determine an optimal trajectory. A pseudospectral method is one of direct-collocation methods, in which the state and control input are expressed as piecewise polynomials, and the collocation points are determined by quadrature rules [17–19]. Using this assumption, we transform the optimal control problem into a nonlinear programming (NLP) problem that already has many efficient solvers. We solve the problems with GPOPS [20], the MATLAB software designed for solving multiphase optimal control problems using the pseudospectral method in [18]. We use the SNOPT [21] as the NLP solver.

A. Descent Profile Simulation

We simulate two aircraft types, B737 and B767, with predetermined flap-speed schedules. In the simulation, the altitudes are specified relative to the mean sea level, and the airspeed constraints in Sec. II are given as CAS instead of IAS. We assume that CAS is equivalent to IAS by ignoring the installation error. The aircraft performance data from the base of aircraft data (BADA) [16] are used in the analysis. However, other general performance data can be used because the formulation is quite general. The predetermined flap-speed schedules are shown in Table 1. The aircraft mass chosen is 52,000 kg for the B737, and 158,800 kg for the B767 based on BADA.

We choose the boundary condition for the numerical examples based on the CDA flight test in Louisville International Airport (KSDF) in [2]. We select a cruise altitude of 35,000 ft and a cruise speed of Mach 0.7818 (265 kt). The maximum allowable descent speed is 350 kt for both B735 and B764. As shown in Table 2, the trajectory optimization starts at the chosen cruise altitude and cruise speed, and terminates at the IAF with an altitude of 3000 ft at a track distance of 8 n mile from the runway threshold and a speed of 180 kt. After this point, the aircraft captures the ILS glide slope and flies the ILS approach. The $d_{\max}$ is set as 150 n mile for both the B735 and the B764. The International Standard Atmosphere conditions are assumed for this simulation, and the air density, pressure, and temperature equations in [16] are used.

B. VNAV CDA

We also compare the optimal trajectories to a reference CDA trajectory generated by the FMS VNAV function. This vertical trajectory was used for a flight test conducted at KSDF in September 2004 [5]. As shown in Fig. 3, the KSDF VNAV CDA profile is determined by a series of VNAV modes. The first segment

Table 2 Initial- and final-point conditions

	Initial condition			Final condition		
Aircraft	H, ft	CAS, kt	Distance, n mile	H, ft	CAS, kt	Distance, n mile
B737	35,000	265	−150	3000	180	−8
B767	35,000	265	−150	3000	180	−8

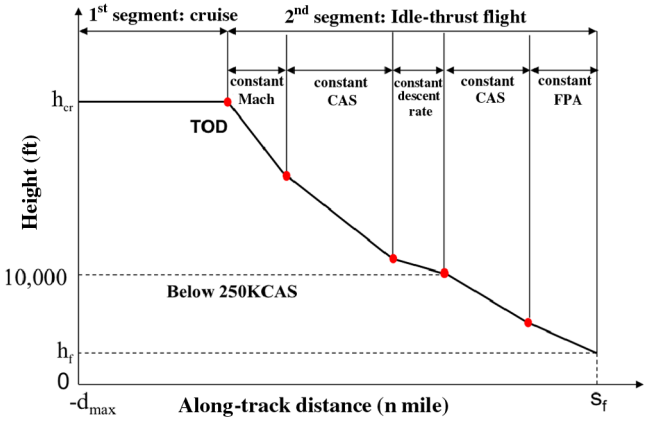

Fig. 3 VNAV CDA trajectory structure.

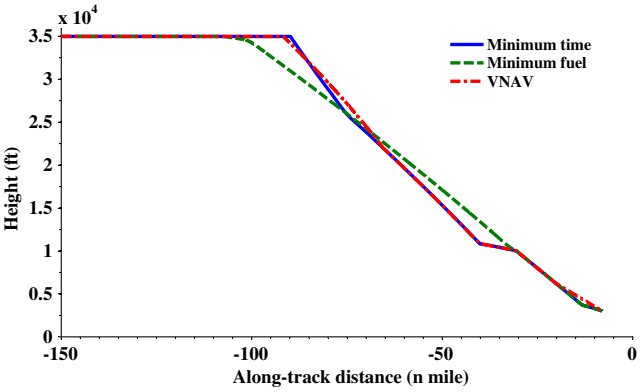

Fig. 4 B737 optimal vertical profiles, zero-wind case.

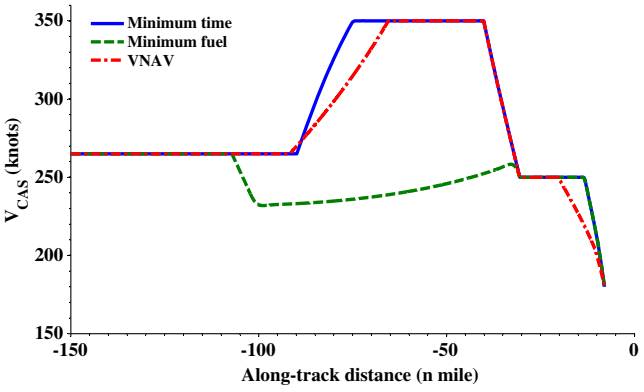

Fig. 5 B737 optimal CAS profiles, zero-wind case.

of this trajectory is the cruise segment. The second segment of the VNAV CDA profile is the idle-thrust segment. In the second segment, the en route part, which is above 10,000 ft, is generated by constant Mach, constant CAS, and constant descent-rate modes [22]. In the en route part, constant Mach/CAS is set to 0.7818/350 based on the KSDF flight test. At the end of the en route part in the second segment, the aircraft attains the FAA regulated speed of 250 kt at 10,000 ft. From that point onward, constant CAS at 250 kt and constant FPA segments are used to satisfy the final-point conditions. The VNAV CDA profile is calculated via backward integration from the final point to the TOD. The mode change between the constant CAS and the constant FPA occurs when the CAS reaches 250 kt during the backward integration from the IAF. By this way, the engine throttle would remain at idle during the entire procedure from the TOD to the final point.

C. B737 Results

The results of the B735 minimum-time and minimum-fuel optimal trajectories are shown in Figs. 4 and 5 along with the VNAV CDA trajectory. For the minimum-time case shown in Fig. 5, the aircraft accelerates until it reaches the 350 kt maximum allowable speed, and then descends at a constant CAS. To satisfy the FAA speed-limit regulation, before 10,000 ft, the aircraft decelerates at the minimum descent rate. Below 10,000 ft, the aircraft flies at the maximum speed of 250 kt as long as possible before decelerating to reach the final speed and altitude conditions. The altitude and speed profiles are determined at the boundaries of several constraints. These characteristics of the minimum-time profile imply that the aircraft flies with maximum performance to reduce flight time.

The minimum-fuel trajectory is quite different from the minimum-time trajectory. For the minimum-fuel trajectory, the aircraft flies with idle power as long as possible; hence, the aircraft starts descending much earlier than in the minimum-time case. From the TOD to 10,000 ft, the aircraft descends with small variations in FPA, as shown in Fig. 4. Furthermore, the speed variation from the TOD to the end point of the first phase is also small. The speed profile is determined to be near 250 kt, which is the maximum allowable speed below 10,000 ft.

Figures 4 and 5 reveal an interesting result. At 10,000 ft, the minimum-fuel and minimum-time trajectories intersect, and are identical below 10,000 ft. This fact means that the noise impact is the same for both optimal trajectories because the noise impact in the vicinity of the airport is a function of the state of aircraft below 10,000 ft. Another important result is that the performance difference between the minimum-time and minimum-fuel trajectories occurs only above 10,000 ft trajectory, which is during the en route descent.

Table 3 reflects the numerical results of the optimal vertical profiles for the B735. As shown in the table, the optimal TOD position in the minimum-time case is 90 n mile from the runway threshold, which is about 18 n mile closer to the runway threshold than the optimal TOD for the minimum-fuel case, which is about 107 n mile from the runway threshold. In addition, if the aircraft flies along the minimum-fuel trajectory, as much as 54 kg fuels can be saved, which is about 11.88% of the total fuel burned in the minimum-time case. On the other hand, if the aircraft flies along the minimum-time trajectory, we can reduce flight time by 178 s, which is a 12.16% reduction in the flight time compared to the flight time needed for the minimum-fuel case. The VNAV CDA case results are very similar to the results of the minimum-time case with a difference in fuel burn of only 5 kg and a flight-time difference of only 20 s. Because the minimum-fuel and minimum-time CDA trajectories consist of the performance bound of the CDA procedure with a given wind condition [13], ATCs or air carriers can improve their benefits by varying the CDA trajectory between two performance limit trajectories.

D. B767 Results

The optimal vertical and speed profiles of a CDA procedure for the B764 with respect to minimum-time and minimum-fuel performance indices are shown in Figs. 6 and 7, respectively. Compared to the B735, the B764 is quite large and heavy; hence, the performance characteristics of the aircraft are quite different from those of the B735. Despite the large differences in the parameters, we can see that the tendencies of the B764 optimal trajectories are very similar to those of the B735 when comparing the trajectories and speed profiles in Figs. 4–7. In the minimum-time case, the optimal CDA speed and altitude profiles for the B764 are determined at the boundaries of the

Table 3 Numerical results of the B737 optimal trajectories

Performance index	TOD, n mile	Fuel burn, kg	Arrival time, s
Minimum time	−90	459	1280
Minimum fuel	−107	405	1458
VNAV CDA	−92	454	1300

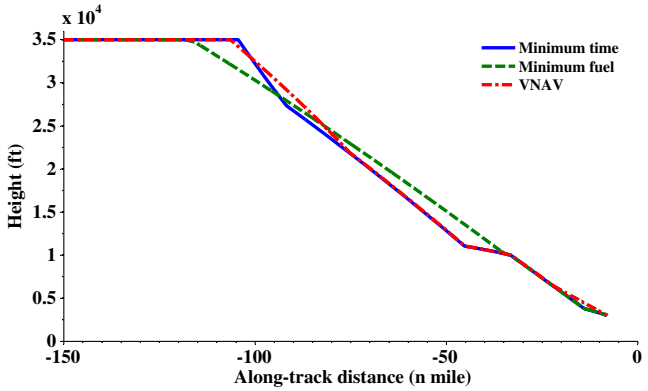

Fig. 6 B767 optimal vertical profiles, zero-wind case.

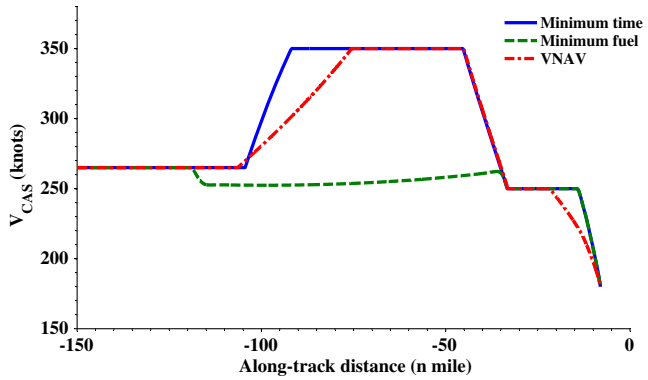

Fig. 7 B767 optimal CAS profiles, zero-wind case.

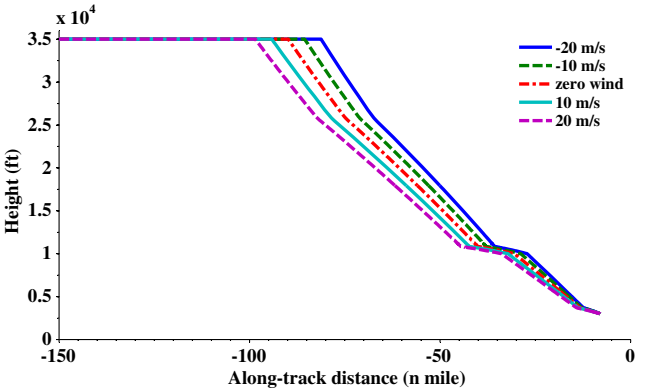

Fig. 8 B737 minimum-time trajectories for different wind conditions.

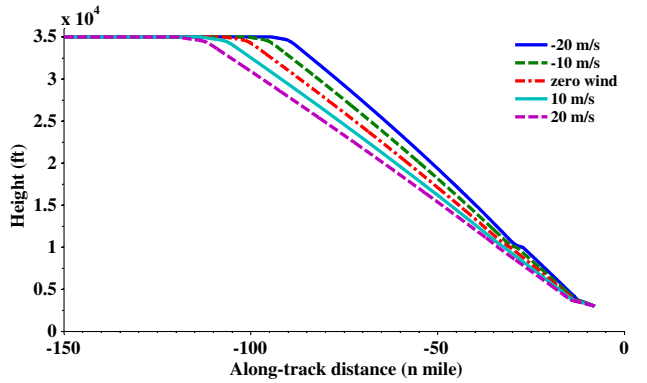

Fig. 9 B737 minimum-fuel trajectories for different wind conditions.

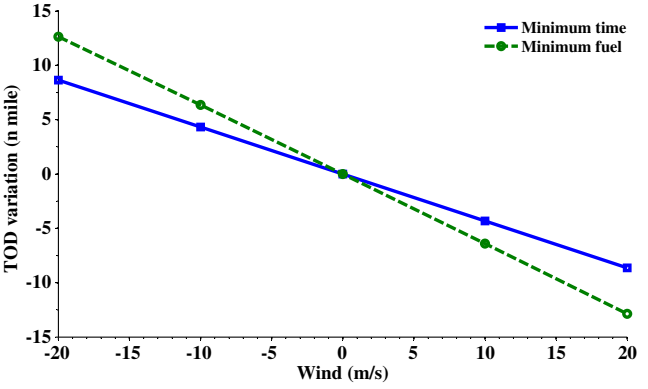

Fig. 10 TOD variations with respect to the wind conditions.

constraints, and this tendency is the same as that for the B735 optimal profiles. The minimum-fuel optimal profiles for the B764 intersect the minimum-time optimal profile at 10,000 ft, and below this point, the optimal profiles of two performance indices are the same as in the B735 case. As in the B735 profiles, the noise impacts below 10,000 ft are identical between the minimum-fuel and minimum-time trajectories.

The numerical values of the optimal vertical profiles for the B764 are shown in Table 4. Flight along the minimum-fuel profile consumes 85 kg less fuel than in the VNAV CDA case, which is an 11.7% fuel savings when compared to the VNAV CDA case. A minimum-time profile can reduce flight time by as much as 23 s when compared to the VNAV CDA case, and 161.32 s when compared to the minimum-fuel case.

E. Effect of Wind

Because the wind profile strongly affects the aircraft trajectory, it is very important to observe the sensitivity of the optimal trajectory with respect to various wind speeds and directions. To observe the wind effect on the optimal trajectory, we performed numerical experiments with various wind speeds and directions. In this study, we consider a wind-speed range from −20 to 20 m/s, in which a negative value denotes a headwind, and a positive value denotes a tailwind.

The effects of wind on the B735 minimum-time and minimum-fuel trajectories are shown in Figs. 8 and 9, respectively. As expected, the TODs in the tailwind cases are more distant than they are in the zero-wind case, and the TODs in the headwind cases are closer than in the zero-wind case. However, the structures of the vertical profile in all wind cases are the same as they are in the zero-wind case. The wind cases also do not alter the relationship between the minimum-time and minimum-fuel vertical profiles. The TOD variations with respect to the wind conditions are shown in Fig. 10 comparison to the zero-wind case. The variations are almost linear for both the minimum-time and -fuel profiles. However, the slope of the TOD variation with wind for the minimum-fuel trajectory is steeper than that for the minimum-time trajectory. This implies that the minimum-fuel optimal profile is more sensitive to wind than the minimum-time optimal profile.

Table 4 Numerical results of the B767 optimal trajectories

Performance index	TOD, n mile	Fuel burn, kg	Arrival time, s
Minimum time	−104	742	1297
Minimum fuel	−119	642	1458
VNAV CDA	−106	727	1320

F. Effect of Cross Wind

To evaluate the cross-wind effects on the optimal trajectory, we compared the case in which the cross-wind term W_c is zero and nonzero W_c case with the same horizontal-wind speed. We simulated three different W_h cases: W_h is zero, 10, and −10 m/s. The wind

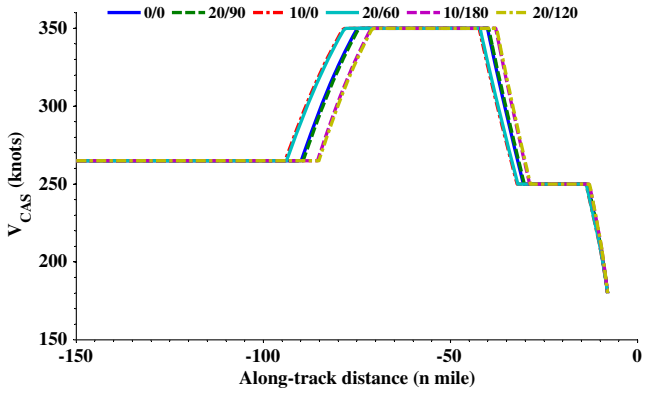

Fig. 11 B737 minimum-time CAS profiles with different cross-wind conditions.

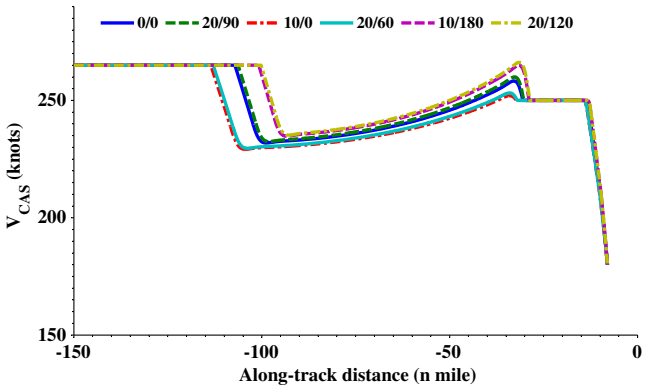

Fig. 12 B737 minimum-fuel CAS profiles with different cross-wind conditions.

vector can be described as a combination of total wind speed and angle $\Psi_w - \psi$ in Fig. 1. For example, (10/90) means the total wind speed is 10 m/s and the $\Psi_w - \psi$ is 90 deg. Therefore, (0/0, 20/90), (10/0, 20/60), and (10/180, 20/120) are the cases in which the W_h is the same each other, but the W_c is different. We compared the results with these wind-speed pairs.

The cross-wind effects on the B735 minimum-time and minimum-fuel CAS profiles are shown in Figs. 11 and 12, respectively. These figures show that the effect of the cross-wind term is relatively smaller than the effect of the horizontal wind in both the minimum-time and minimum-fuel cases.

G. Effect of Wind Shear

To evaluate the wind-shear effect on the optimal trajectory, we solved the optimal control problem with the following nominal wind model:

$$W = A_0\left(\frac{h}{h_0}\right)^{A_1} \tag{22}$$

in which A_0 is the wind at h_0, and A_1 represents the wind-shear-effect terms. We used the four different wind conditions; (A_0, A_1) are (20, 0), (20, 1/7), (20, 3/7), and (20, 1). Here, we used the cruise altitude as h_0, and hence A_0 is the wind speed at the cruise altitude.

The wind-shear effects on the B735 optimal CAS profiles are shown in Fig. 13. The CAS profiles in the minimum-time cases are the same regardless of different wind-shear terms, as shown in Fig. 13b. The minimum-time CAS profiles in all cases are generated on the boundaries of the path constraints. In the minimum-fuel case in Fig. 13c, the CAS profiles are not exactly the same, but they are very similar to each other. This observation means that wind-shear effects on the minimum-fuel trajectories are small, and the dominant wind term is the wind speed at the cruise altitude, as shown in Figs. 9 and 12.

IV. Suboptimal VNAV Trajectory Strategy

In the current CDA arrival procedures, the vertical flight path and speed profile are calculated by the FMS using VNAV descent algorithms that have been in use for over two decades. For this reason, an arrival procedure with the FMS-generated trajectory can produce many benefits, including enhancement of both the pilot's and controller's situational awareness, and, therefore, enhanced safety. Thus, even though some performance degradation may occur when compared to arrivals flying the optimal trajectories obtained in Sec. III, a VNAV CDA procedure can have many benefits from a practical-implementation point of view.

In this section, we present suboptimal VNAV CDA trajectories in terms of minimum flight time and minimum-fuel consumption. The suboptimal VNAV trajectories are divided into several segments, and each segment is built with existing VNAV descent algorithms. VNAV descent algorithms are categorized in terms of constant CAS/Mach mode, constant FPA mode, and constant ROD mode [22]. Because the flight idle-thrust setting is assumed for the purpose of reducing the noise impact, the same as with optimal trajectories in Sec. III, the VNAV CDA trajectories are typically built with idle-thrust

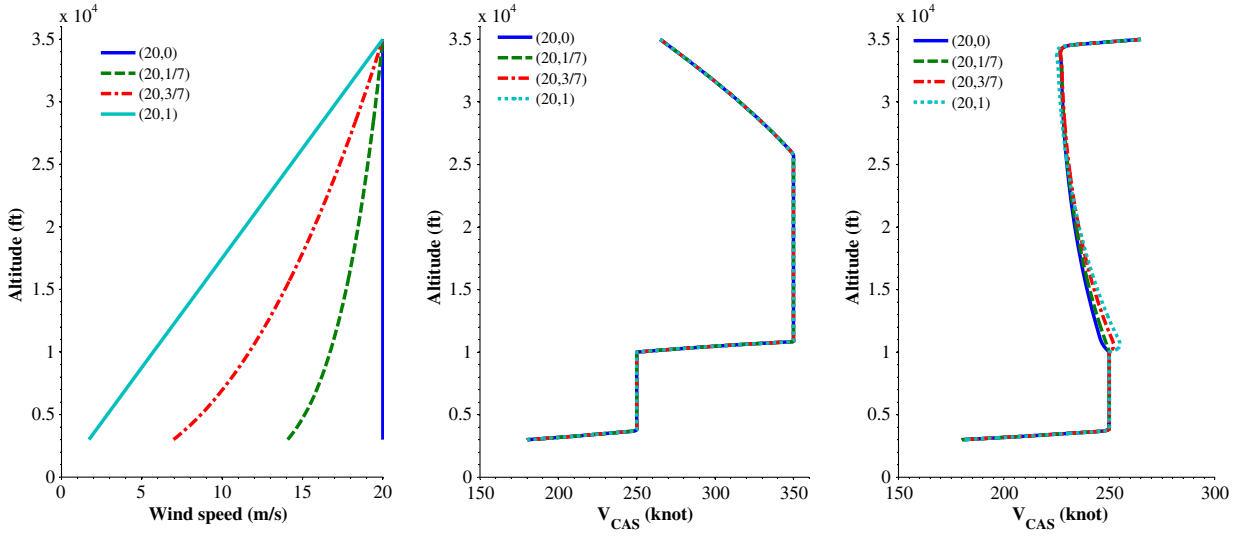

a) Wind **b) Minimum time** **c) Minimum fuel**

Fig. 13 B737 optimal CAS profiles with different wind-shear conditions.

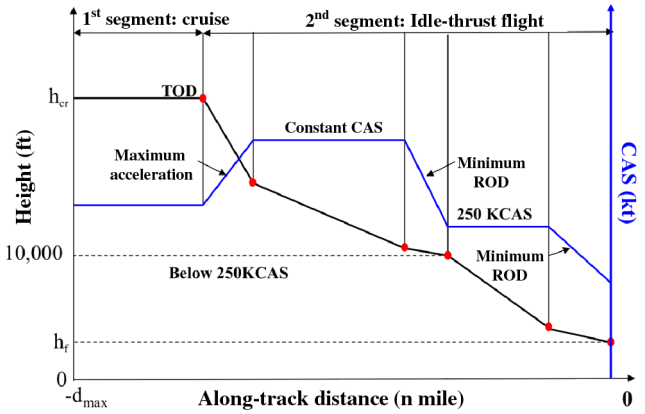

Fig. 14 Proposed minimum-time VNAV altitude and speed profiles.

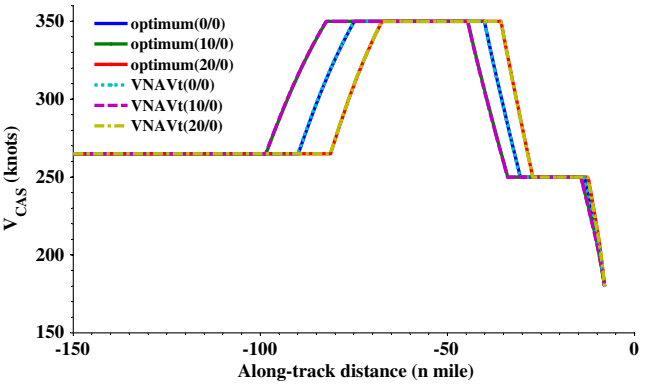

Fig. 15 B737 minimum-time CAS: true optimum and VNAV cases.

assumption. Hence, each mode calculates the FPA, which is the control input in the trajectory-optimization problem.

A. Minimum-Time Suboptimal VNAV CDA

In both the B735 and B764 cases in Sec. III, the minimum-time speed profiles are determined at the maximum performance bounds, such as the maximum ROD, the maximum FPA, and the maximum CAS, as shown in Figs. 5 and 7. From this observation, we propose the minimum-time suboptimal VNAV CDA trajectory structure, as shown in Fig. 14.

The proposed minimum-time VNAV CDA suboptimal speed profile consists of two segments: a cruise segment and a flight idle-descent segment. The idle-descent segment is generated by forward and backward integration using the VNAV mode sequence: maximum acceleration–constant Mach/CAS–minimum ROD–constant CAS of 250 kt–minimum ROD. The first component of the second segment in Fig. 14, which is the maximum acceleration mode, starts at the TOD and is generated by the forward integration with the CAS increasing during this portion of the descent. Depending on the initial speed, this component can be generated by using either one of two modes, the maximum descent-rate mode or the fixed FPA mode, or by using both modes. From the descent-rate constraint in Eq. (18) and the control-input constraint in Eq. (21), the aerodynamic FPA for maximum acceleration is given by

$$\gamma = \max[\sin^{-1}(\dot{h}_{\min}/V_T), \gamma_{\min}] \tag{23}$$

The VNAV CDA trajectory from the second component of the flight idle-descent segment to the last component in Fig. 14 is generated by backward integration. The second component starts at the point where the CAS reaches the maximum allowable CAS and continues to fly at this CAS as long as possible. If the airspeed reaches the maximum allowable Mach before reaching the maximum CAS, the constant Mach mode with the maximum value should be inserted between the first and second segments in Fig. 14. At the end of the second component, the aircraft decelerates using the minimum descent rate until reaching 250 kt, which is the maximum speed below 10,000 ft as stipulated by the FAA regulation. The rest of the trajectory below 10,000 ft is similar to the upper trajectory. Because the maximum allowable speed is 250 kt below 10,000 ft, the speed constraint in Eq. (17) is active. Therefore, the third component is generated using constant CAS. The last component is at the minimum descent rate to decelerate to the final-point speed restriction at the specified altitude.

B. Numerical Results of the Minimum-Time VNAV CDA

To evaluate the VNAV CDA trajectory with various wind conditions, we compared three wind-condition cases: (0/0), (10/0), and (20/0). The first number means the total wind speed in meters per second, and the second number means $\Psi_w - \psi$ in degrees. The minimum-time CAS profile comparisons between an optimal minimum-time CDA and a suboptimal VNAV CDA built as described previously are shown in Figs. 15 and 16. In both cases, the VNAV results are the same as the optimal results. Because the minimum-time optimal trajectories are determined by the aircraft performance bounds, such as speed limit, ROD limit, and control-input limit, the minimum-time trajectories can be generated by the combination of VNAV algorithms.

C. Minimum-Fuel Suboptimal VNAV CDA

While the minimum-time VNAV CDA trajectory is easily built using the general aspects of the minimum-time optimal control problem, the minimum-fuel VNAV CDA profile cannot be determined intuitively because the profile is not determined by the boundaries of the constraints. Therefore, generating an identical profile using a combination of VNAV descent algorithms is impossible. Hence, we need to simplify the optimal profile considering the characteristics of the minimum-fuel profiles.

Because the profiles below 10,000 ft are the same for both the minimum-time and minimum-fuel profiles, we can build the same minimum-fuel VNAV profile with the minimum-time VNAV profile, which consists of the following series of VNAV modes: constant CAS with 250 kt–constant ROD with minimum value. The problem is en route descent part, which is the area above 10,000 ft. As shown in Figs. 5 and 7, the minimum-fuel descent profiles are not determined by the boundaries of the path constraints. Therefore, we must approximate the en route descent profile with a series of VNAV modes. In this paper, we use constant ROD–constant CAS–constant ROD for the en route trajectory generation because constant Mach/CAS descent is used for the current VNAV CDA trajectory generation [2,5]. The overall structure of the minimum-fuel VNAV CDA trajectory is shown in Fig. 17.

Because the minimum-fuel VNAV profile is simple and most of the descent is at a constant speed, the proposed VNAV trajectory has the benefit of pilot controllability. With the proposed VNAV profile, the procedure is executed and controlled by the FMS, which monitors the progress of the planned descent both laterally and vertically. Control inputs are not required by the pilot unless the FMS senses that

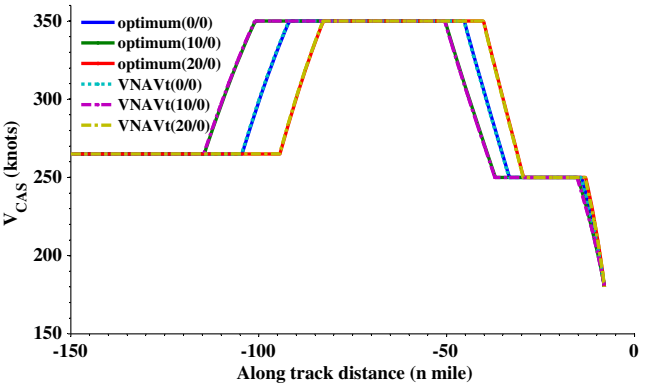

Fig. 16 B767 minimum-time CAS: true optimum and VNAV cases.

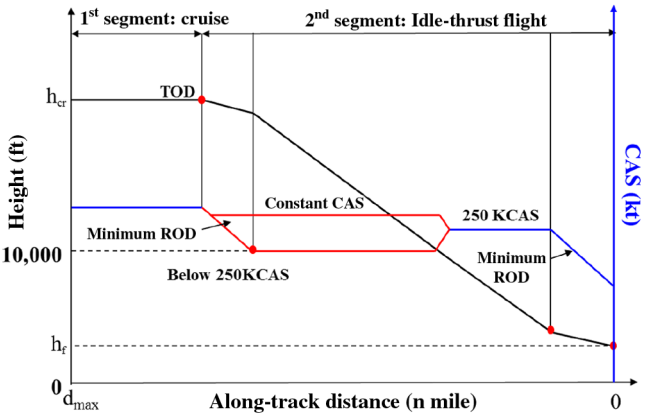

Fig. 17 Proposed VNAV minimum-fuel trajectory and speed profile.

the aircraft cannot maintain the desired trajectory within its control capability, and prompts the pilot that a specific action is needed to maintain the profile.

The minimum-fuel VNAV CDA trajectory-optimization problem in Fig. 17 can be solved by modifying the original optimal control problem described in Sec. II. By using the VNAV mode sequence for the minimum-fuel en route descent profile, we divide the en route descent phase of the idle-thrust segment in Fig. 1 into three phases: constant ROD, constant CAS, and constant ROD. The ROD values of the first and third phases are determined by the CAS value in the second phase. If the optimal CAS in the second phase is lower than the cruise speed, the first ROD is set to the minimum ROD value to decelerate. On the other hand, the ROD is set to the maximum value to accelerate if the CAS in the second phase is larger than the cruise speed. The ROD at the third phase is determined by comparing the optimal CAS with 250 kt, which is the CAS at 10,000 ft. Then, the minimum-fuel VNAV CDA trajectory can be described by only one parameter, which is the CAS value in the second phase. Therefore, the original optimal control problem can be converted to the following parameter-optimization problem:

$$\min J(V_{\mathrm{CAS}}) \quad V_{\mathrm{min,CAS}} \le V_{\mathrm{CAS}} \le V_{\mathrm{max,CAS}} \tag{24}$$

D. Numerical Results of the Minimum-Fuel VNAV CDA

Evaluating the performance of the proposed minimum-fuel VNAV profile requires a comparison with the minimum-fuel optimal profile. Because the minimum VNAV CDA trajectory-optimization problem in Eq. (24) is the parameter-optimization problem with only one parameter, it can be solved very easily using the NLP solvers. In this section, we used an interior-point method to solve this optimization problem.

The altitude- and speed-profile comparisons between the minimum-fuel optimal CDA and the proposed VNAV CDA are shown in Figs. 18 and 19. Although the speed profiles above 10,000 ft of the proposed VNAV trajectory are different from the optimal profile, we can observe that the altitude profiles of the proposed VNAV trajectory are similar for all wind cases. The CAS determined by the parameter optimization is very close to the average CAS of the en route descent segment of the true optimal trajectory in Sec. III.

The characteristics of the minimum-fuel VNAV CDA are documented in Tables 5 and 6. As expected, there is performance degradation with regard to fuel consumption. This degradation may have occurred due to the differences in the speed profiles. Because the TOD points of the VNAV trajectories are smaller than those of the true optimal trajectories for all wind cases for both aircraft, the fuel burns of the VNAV trajectories during the cruise are smaller than

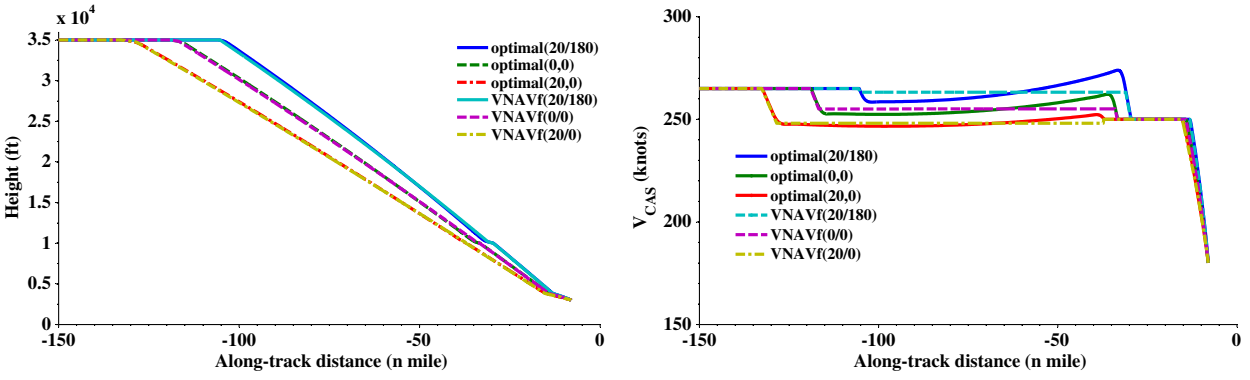

a) Altitude b) CAS

Fig. 18 B767 minimum-fuel-trajectory comparison of optimal and VNAV suboptimal results.

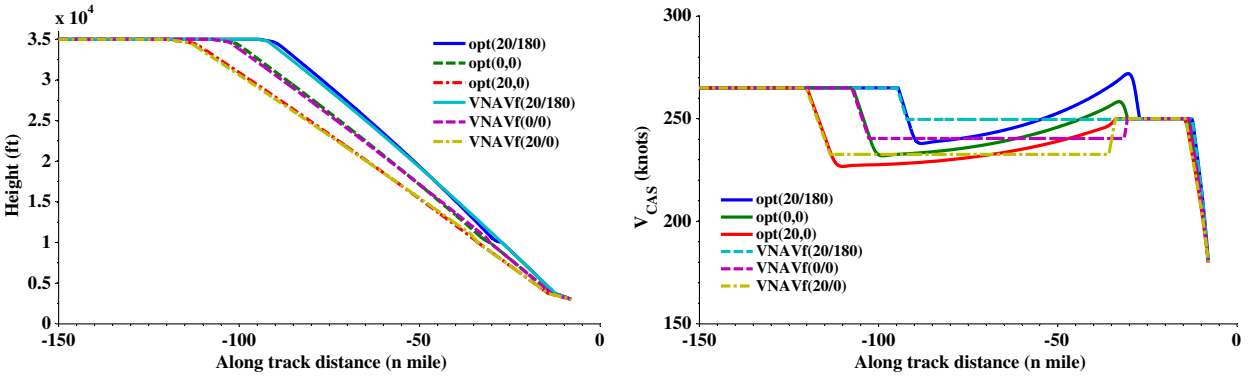

a) Altitude b) CAS

Fig. 19 B737 minimum-fuel-trajectory comparison of optimal and VNAV suboptimal results.

Table 5 Numerical comparison of the B767 VNAV trajectories

	True optimal			VNAV suboptimal		
Wind (W/ψ_w)	Time, s	Fuel, kg	TOD, n mile	Time, s	Fuel, kg	TOD, n mile
(20, 180)	1570	825	−105	1574	825	−106
(0, 0)	1458	642	−119	1461	643	−119
(20, 0)	1363	486	−133	1363	486	−133

Table 6 Numerical comparison of the B737 VNAV trajectories

	True optimal			VNAV suboptimal		
Wind (W/ψ_w)	Time, s	Fuel, kg	TOD, n mile	Time, s	Fuel, kg	TOD, n mile
(20, 180)	1566	494	−95	1573	495	−94
(0, 0)	1457	405	−107	1464	405	−107
(20, 0)	1363	328	−120	1368	328	−120

those of the true optimal trajectories. Therefore, the fuel-burn difference between the true optimal and VNAV suboptimal trajectories comes from the descent segment.

In the B735 case, the maximum difference among the three wind cases is 1 kg in fuel and 7 s in flight time. In the B764 case, the maximum difference in fuel consumption between the two trajectories is less than 1 kg. As these numerical results show, we can observe that the performance degradation that results from simplifying the speed profile is very small. Therefore, by using the proposed VNAV profile, we can obtain many practical benefits of a VNAV approach while introducing only very small performance degradation when compared to the optimal trajectory.

The optimal CAS values of the B735 and the B764 for the en route descent with different wind conditions are shown in Fig. 20. The optimal CAS values vary as the wind speed at cruise altitude changes. The optimal CAS decreases as the tailwind increases. However, the parameter A_1 in the nominal wind model in Eq. (22) does not affect the optimal CAS values. This result means that the optimal CAS value is more sensitive to A_0, which is the wind speed at the cruise altitude, than the wind-shear term A_1. This result is very similar to the result of the wind-shear effects in Sec. III.G.

The cross-wind effects on the optimal CAS values of the B735 and the B764 are shown in Fig. 21. The variation of the optimal CAS due to the cross wind is much smaller than the variation due to the horizontal wind.

From the preceding results, we found that the horizontal-wind speed at the cruise altitude is the most dominant factor to determine the optimal CAS value for the minimum-fuel VNAV CDA trajectory with the given structure in Fig. 17. As shown in Figs. 20 and 21, the differences of the optimal CAS when compared to the constant horizontal-wind case are less than 3 kt for all tested wind conditions. Furthermore, the optimal CAS values can be approximated by a quadratic equation with respect to the horizontal-wind speed at the cruise altitude. Therefore, if the FMS has this approximated equation, then the FMS can generate minimum-fuel VNAV CDA trajectory close to the true optimal trajectory without solving the optimization problem in Eq. (24). The approximated optimal CAS value functions for the B735 and the B764 are as follows:

$$V_{\mathrm{CAS}}^{\mathrm{opt}} = \begin{cases} 2.0305\times10^{-3}W_h^2 - 0.4255W_h + 240.33 & \text{if } B737-500 \\ 1.5544\times10^{-3}W_h^2 - 0.3770W_h + 255.05 & \text{if } B767-400 \end{cases} \tag{25}$$

E. Computational-Time Comparison

Computational load is the one of the critical issues to implement the proposed trajectory-generation method in the FMS or ground automation tools. To evaluate the benefits of the proposed suboptimal VNAV trajectory-generation method, we compared the total computational times of three different methods: 1) optimal control technique using GPOPS in Sec. III, 2) suboptimal VNAV trajectory generation by solving the parameter-optimization problem in Eq. (24), and 3) suboptimal VNAV solution using the approximated speed equation in Eq. (25). For the comparison, the B735 with the zero-wind case in Sec. III was selected. The computational time was measured on an AMD Athlon II Dual-Core M320, 2.1 GHz, 3.0 GB RAM HP laptop with MATLAB R2010b implementation. The comparison result is shown in Table 7.

In the minimum-time case, we do not need to solve the parameter-optimization problem because the minimum-time trajectory is determined at the performance boundary with existing VNAV mode, as shown in Sec. IV.A. In the minimum-fuel case, by using the proposed suboptimal VNAV methods, which are methods 2 and 3, we can reduce the computational time significantly while keeping the almost same performance, as shown in Sec. IV.D.

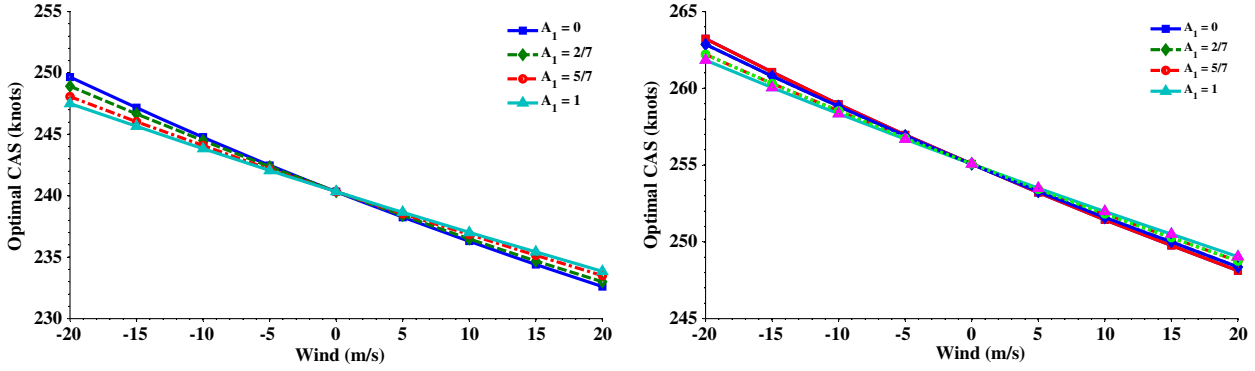

a) B737-500 b) B767-400

Fig. 20 Minimum-fuel CAS with various wind-shear conditions.

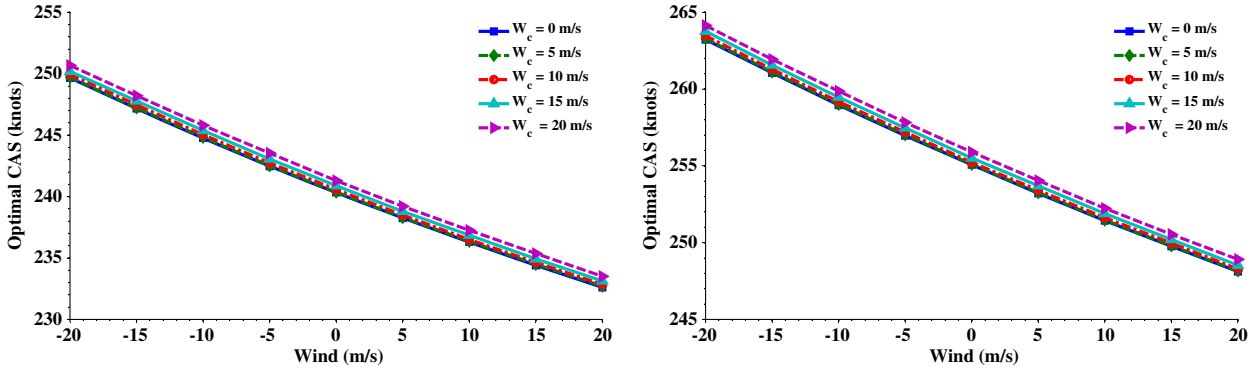

Fig. 21 Minimum-fuel CAS with various cross-wind conditions.

V. Conclusions

A CDA procedure is beneficial in that its application can reduce operating costs by reducing the flight time and fuel burn, and has the environmental benefits of reducing noise and gaseous emissions. To maximize these benefits, a CDA trajectory optimization problem with a specified range was formulated, which includes a part of the cruise segment. The CDA trajectory optimization formulation was aided by a multiphase optimal control problem framework. Each phase was divided according to the flap-speed schedule and the FAA speed-limit regulation. By establishing a free condition at the initial along-track distance, both an optimal TOD position and a descent trajectory were simultaneously obtained.

The formulated multiphase optimal control problems were solved using a pseudospectral method for two aircraft types: the B737 and the B767. The various numerical results presented here have led to an understanding of the characteristics of the optimal trajectories with respect to flight time and fuel consumption. The two optimal trajectories are identical below 10,000 ft, whereas the speed and altitude profiles of the en route descent part are quite different. This result means that the possible performance variations come from the en route descent part.

Based on this analysis of true optimal trajectories, the VNAV mode sequence for both the minimum-time and minimum-fuel cases was found. By using these fixed mode sequences, the suboptimal VNAV CDA profiles with objective functions of the minimum flight time and minimum-fuel consumption were built. Because the proposed VNAV CDA profiles can be calculated by onboard FMS computer without additional equipment, they represent a practical implementation. In the minimum-time case, all segments of the optimal trajectory are determined at the boundary of the constraints, and the proposed VNAV CDA profile is constructed with the aircraft descending under the maximum allowable operating conditions. The resulting performance of the VNAV CDA profile was identical to the optimal results. In the minimum-fuel case, the suboptimal VNAV trajectory problem was converted to the parameter-optimization problem, and the optimal CAS was calculated with different wind cases. The numerical results showed that the dominating factor in determining the optimal CAS is the horizontal speed at cruise altitude. Based on this result, the optimal CAS value functions were approximated using quadratic formulation.

The analysis result and the proposed VNAV trajectory generation method can be applied in both ground and airborne automation systems. If the aircraft has the capability to calculate the parameter optimization, using the proposed VNAV sequence, the optimal trajectory can be calculated very quickly, and hence, realize the online trajectory planning. The alternative way is that a ground automation tool solves the parameter-optimization problem using the proposed VNAV sequence, and sends the optimal parameter to the aircraft via data link.

Another application of this study is the decision-supporting tool to determine the optimal scheduling of the traffic flow to the runway. To determine the optimal scheduling, which is the RTA, an ATC should know the performance bound of the individual aircraft, such as the feasible time range of the CDA flight. This study provides the methodology to analyze the performance bound of individual aircraft. The performance-bound-analysis results can be used as constraints of the optimal scheduling problem.

Table 7 Computational-time comparison

Performance index	Computational times, s		
	Method 1 (GPOPS)	Method 2 [Eq. (24)]	Method 3 [Eq. (25)]
Minimum time	10.91	— —	1.80
Minimum fuel	53.16	3.53	1.79

References

[1] Clarke, J.-P. B., "Systems Analysis of Noise Abatement Procedures Enabled by Advanced Flight Guidance Technology," *Journal of Aircraft*, Vol. 37, No. 2, 2000, pp. 266–273. doi:10.2514/2.2590

[2] Clarke, J.-P. B., Ho, N. T., Ren, L., Brown, J. A., Elmer, K. R., Zou, K., Hunting, C., McGregor, D. L., Shivashankara, B. N., Tong, K.-O., Warren, A. W., and Wat, J. K., "Continuous Descent Approach: Design and Flight Test for Louisville International Airport," *Journal of Aircraft*, Vol. 41, No. 5, 2004, pp. 1054–1066. doi:10.2514/1.5572

[3] Reynolds, T. G., Ren, L., and Clarke, J.-P. B., "Advanced Noise Abatement Approach Activities at a Regional UK Airport," *Air Traffic Control Quarterly*, Vol. 15, No. 4, 2007, pp. 275–298.

[4] Ren, L., and Clarke, J.-P. B., "Separation Analysis Methodology for Designing Area Navigation Arrival Procedures," *Journal of Guidance, Control, and Dynamics*, Vol. 30, No. 5, 2007, pp. 1319–1330. doi:10.2514/1.27067

[5] Ren, L., and Clarke, J.-P. B., "Flight-Test Evaluation of the Tool for Analysis of Separation and Throughput," *Journal of Aircraft*, Vol. 45, No. 1, 2008, pp. 323–332. doi:10.2514/1.30198

[6] Erzberger, H., and Lee, H., "Constrained Optimum Trajectories with Specified Range," *Journal of Guidance, Control, and Dynamics*, Vol. 3, No. 1, 1980, pp. 78–85. doi:10.2514/3.55950

[7] Sorensen, J. A., and Waters, M. H., "Airborne Method to Minimize Fuel with Fixed Time-of-Arrival Constraints," *Journal of Guidance, Control, and Dynamics*, Vol. 4, No. 3, 1981, pp. 348–349. doi:10.2514/3.56086

[8] Burrows, J. W., "Fuel-Optimal Aircraft Trajectories with Fixed Arrival Times," *Journal of Guidance, Control, and Dynamics*, Vol. 6, No. 1, 1983, pp. 14–19. doi:10.2514/3.19796

[9] Chakravarty, A., "Four-Dimensional Fuel-Optimal Guidance in the Presence of Winds," *Journal of Guidance, Control, and Dynamics*, Vol. 8, No. 1, 1985, pp. 16–22. doi:10.2514/3.19929

[10] Visser, H. G., and Wijnen, R. A., "Optimisation of Noise Abatement Arrival Trajectories," *Aeronautical Journal*, Vol. 107, No. 1076, 2003, pp. 607–616.

[11] Slattery, R., and Zhao, Y., "Trajectory Synthesis for Air Traffic Automation," *Journal of Guidance, Control, and Dynamics*, Vol. 20,

No. 2, 1997, pp. 232–238.
doi:10.2514/2.4056

[12] Zhao, Y., and Slattery, R. A., "Capture Conditions for Merging Trajectory Segments to Model Realistic Aircraft Descents," *Journal of Guidance, Control, and Dynamics*, Vol. 19, No. 2, 1996, pp. 453–460. doi:10.2514/3.21639

[13] Park, S. G., and Clarke, J.-P. B., "Feasible Time Range Analysis of Wide Fleet for Continuous Descent Arrival," *AIAA Aviation Technology, Integration and Operations (ATIO) Conference*, AIAA Paper 2013-4229, 2013.

[14] Park, S. G., and Clarke, J.-P. B., "Vertical Trajectory Optimization for Continuous Descent Arrival Procedure," *AIAA Guidance, Navigation, and Control Conference*, AIAA Paper 2012-4757, Aug. 2012.

[15] Ho, N. T., and Clarke, J.-P. B., "Methodology for Optimizing Parameters of Noise-Abatement Approach Procedures," *Journal of Aircraft*, Vol. 44, No. 4, 2007, pp. 1168–1176. doi:10.2514/1.22292

[16] Nuic, A., "User Manual for the Base of Aircraft Data (BADA) Revision 3.6," EUROCONTROL Experimental Centre Technical/Scientific, Rept. 2004-022, Brétigny-sur-Orge, France, Sept. 2004.

[17] Fahroo, F., and Ross, I. M., "Direct Trajectory Optimization by a Chebyshev Pseudospectral Method," *Journal of Guidance, Control, and Dynamics*, Vol. 25, No. 1, 2002, pp. 160–166. doi:10.2514/2.4862

[18] Garg, D., Patterson, M., Hager, W. W., Rao, A. V., Benson, D. A., and Huntington, G. T., "A Unified Framework for the Numerical Solution of Optimal Control Problems Using Pseudospectral Methods," *Automatica*, Vol. 46, No. 11, 2010, pp. 1843–1851. doi:10.1016/j.automatica.2010.06.048

[19] Huntington, G. T., "Advancement and Analysis of Gauss Pseudospectral Transcription for Optimal Control Problems," Ph.D. Dissertation, Dept. of Aeronautics and Astronautics, Massachusetts Inst. of Technology, Cambridge, MA, 2007.

[20] Rao, A. V., Benson, D. A., Darby, C., Patterson, M. A., Francolin, C., Sanders, I., and Huntington, G. T., "Algorithm 902: GPOPS, a MATLAB Software for Solving Multiple-Phase Optimal Control Problems Using the Gauss Pseudospectral Method," *ACM Transactions on Mathematical Software*, Vol. 37, No. 2, 2010, pp. 22:1–22:39. doi:10.1145/1731022

[21] Gill, P. E., Murray, W., and Saunders, M. A., "SNOPT: An SQP Algorithm for Large-Scale Constrained Optimization," *SIAM Journal on Optimization*, Vol. 12, No. 4, 2002, pp. 979–1006. doi:10.1137/S1052623499350013

[22] Ren, L., Ho, N. T., and Clarke, J.-P. B., "Workstation Based Fast-Time Aircraft Simulator for Noise Abatement Approach Procedure Study," *AIAA Aviation Technology, Integration, and Operations (ATIO) Conference*, AIAA Paper 2004-6503, 2004.